Ground-state interpretation of x-ray emission spectroscopy on adsorbates: CO adsorbed on Cu(100)

A. Föhlisch,* J. Hasselström, P. Bennich, N. Wassdahl, O. Karis, and A. Nilsson
Department of Physics, Uppsala University, Box 530, S-751 21 Uppsala, Sweden

L. Triguero, M. Nyberg, and L. G. M. Pettersson
FYSIKUM, University of Stockholm, Box 6730, S-113 85 Stockholm, Sweden

(Received 1 June 1999; revised manuscript received 15 February 2000)

The application of resonant inelastic x-ray scattering and resonantly excited x-ray emission to adsorbates has evolved into a powerful technique to investigate the valence electronic structure of adsorbates in an atom-specific and orbital-symmetry-selective way. A surprisingly simple interpretation of spectral features in a one-electron ground-state interpretation has been found empirically. In this work $c(2\times2)$CO/Cu(100) is used as a prototypical system to investigate and rationalize the ground-state interpretation for adsorbates on metal surfaces, employing experimental data and *ab initio* calculations in different approximations. We conclude that the observed agreement between experiment and the one-electron ground-state interpretation could be due to a cancellation of dynamic core-hole effects and valence-hole relaxation. This hypothesis should be tested further by improving theoretical techniques to include the fully relaxed valence-hole final states, not possible for adsorbate systems at present. An alternative interpretation is that the inelastic x-ray scattering process is a true one-step process without the formation of a relaxed core-hole intermediate state and small differential final-state effects. In any case, resonant inelastic x-ray scattering and resonantly excited x-ray emission applied to adsorbates can be interpreted as an atom-specific and orbital-symmetry-selective projection of the ground-state electronic structure.

I. INTRODUCTION

The description of chemical bonding at surfaces on an atomic level has been the focus of modern surface science, and a detailed understanding of the surface chemical bond requires the determination and interpretation of the adsorbate electronic structure.[1,2] X-ray fluorescence stimulated by electron bombardment or x-ray absorption has long been used as a powerful method to probe the electronic structure of bulk samples due to the large mean free path of the emitted (and incident) x-ray photons. For surface studies the large probe depth was adverse to detecting and separating a signal of comparatively few adsorbed species from the much larger number of substrate atoms. To study the electronic structure of adsorbates, valence-band or ultraviolet photoemission spectroscopy (UPS) became the method of choice.[3] In UPS the mean free path of the outgoing photoelectron is significantly shorter, thus allowing one to separate contributions from adsorbed species from the substrate signal. However, UPS also often suffers from a dominating photoemission signal of the substrate (e.g., transition metals), making a detailed analysis of overlapping adsorbate states difficult.

With the advent of tunable high brilliance third-generation synchrotron light sources of defined polarization, previously impossible experiments with x-ray fluorescence on adsorbates became possible as the valence electronic structure of well-ordered chemisorption systems on metals could be probed atom specifically and orbital symmetry selectively.[4–22] X-ray fluorescence has been made surface sensitive by performing in grazing-incidence resonant inelastic x-ray scattering at the x-ray-absorption edges of atomic centers in the adsorbate species. As the incident photon energy is selectively tuned to the absorption resonance of one atomic center at a time, a core vacancy at this atomic center is created and the resulting resonantly excited x-ray emission is an atom-specific probe of the local electronic structure of the adsorbed molecules. A negligible contribution comes from the much larger number of atoms in the substrate,[4] finally overcoming the limitations of UPS. Since the decay process in x-ray emission is dipole dominated and the transition is governed by the overlap with the core orbital, only information on specific angular momentum contributions is obtainable; i.e., with an intermediate 1*s* core hole only the *p* contributions to the occupied valence orbitals from the specific atom are present.

Parallel to the increasing availability of resonantly excited x-ray emission spectra on adsorbates, the computational description of the x-ray emission spectra of free molecules and adsorbates has undergone a rapid evolution.[23,24] The calculation of the x-ray emission transition moments from ground-state orbitals is in good agreement with experiment for a large variety of systems, e.g., N_2/Ni(100),[10] NH_3/Cu(110),[14] NO/Ru(001),[15] ethylene and benzene on Cu(110),[16,17] CO adsorption,[18–20] and formate, acetate, and glycine on Cu(110).[21,22] This is somewhat surprising—and will be discussed in detail—as these ground-state calculations represent just the most simple one-electron picture of a passive core hole into which the ground state valence electrons decay. The use of transition potentials (i.e., a half-occupied core hole[25,26]) or fully relaxed core-hole states has been shown not to necessarily improve the description.[16] Furthermore, for adsorbates on strongly correlated substrates, e.g., transition metals, density-functional theory (DFT) has been found favorable to Hartree-Fock-based ap-

proaches to calculate the ground-state electronic structure using, e.g., a cluster description.

In this study we investigate and rationalize the one-electron ground-state interpretation of resonant inelastic x-ray scattering and resonantly excited x-ray emission on adsorbates on transition- and noble-metal surfaces. Most important in this discussion is the connection between the relative intensities in the spectral distribution and the atomic populations in the adsorbate electronic structure. In addition, the ground-state interpretation of the spectroscopic observables in a one-electron picture requires a thorough discussion of the spectroscopic process, investigating the role of core-hole creation and annihilation and the presence of valence-vacancies, vibrational excitations, and the long-range order of the adsorbate.

We have chosen $c(2\times2)$CO/Cu(100) as the prototype system from the large number of systems investigated by us,[4–22] as it is well known experimentally and computationally. As a result we find that many aspects of the ground-state interpretation of resonantly excited x-ray emission spectroscopy are directly linked to the metallic character of the adsorbate systems. $c(2\times2)$CO/Cu(100) is rather weakly coupled (adsorption energy 0.7 eV/molecule[27]), but its valence electronic structure still has metallic character and its dynamic response to core-hole creation is characterized by dynamic metallic screening.[28,31,34] The argumentation valid for $c(2\times2)$CO/Cu(100) as the limiting, weakly coupled case is therefore certainly applicable to all the adsorbate systems with stronger coupling.

II. GENERAL CONSIDERATIONS

A. Resonant inelastic x-ray scattering and resonantly excited x-ray emission

The concept of resonant inelastic x-ray scattering (RIXS) in general and the specific case of resonantly excited x-ray emission (XES) play central roles in our discussion geared toward adsorbates. RIXS describes the inelastic scattering of x rays, with the photon energy tuned to the x-ray-absorption resonance of the scatterer, where the resonant inelastic scattering cross section is given in perturbational treatment by the modified Kramers-Heisenberg formula:[24,29]

$$I_{RIXS}(\omega',\omega)\propto\sum_F\left|\sum_M\frac{\langle F|\vec{D}\cdot\vec{E'}|M\rangle\langle M|\vec{D}\cdot\vec{E}|G\rangle}{\hbar\omega-(E_M-E_F)+i\Gamma_M/2}\right|^2\times\delta(\hbar\omega-\hbar\omega'+E_G-E_F). \quad (1)$$

The energy of the incoming and outgoing photons is given by $\hbar\omega$ and $\hbar\omega'$, with the electric-field vectors $\vec{E}$ and $\vec{E'}$, respectively. The scattering process consists of x-ray absorption from the ground state $|G\rangle$ to intermediate states $|M\rangle$, and x-ray emission to all final states $|F\rangle$ with energies E_G, E_M, and E_F, respectively. The core-hole intermediate states have a lifetime broadening Γ_M. For different core-hole intermediate states with an energetic separation comparable to their lifetime broadening Γ_M, the multiple-scattering channels interfere, making the x-ray absorption and x-ray emission inseparable.[24] The interfering intermediate states are due to closely spaced absorption resonances or vibrational excitations. In the RIXS process the initial and final states transform according to the same irreducible representation, where the total nuclear and electronic symmetry of the scatterer has to be considered, since the nuclear and electronic motion is coupled.

Resonantly excited x-ray emission is the special case of RIXS, where only a single core-hole intermediate state $|M\rangle$ is reached. Then RIXS can be described as an independent x-ray-absorption step and subsequent radiative decay of the core-hole state, which we denote as resonantly excited x-ray emission (XE). The x-ray emission cross section is then given by Fermi's golden rule:

$$I_{XE}(\omega')\propto\sum_F(E_M-E_F)^3|\langle F|\vec{D}\cdot\vec{E'}|M\rangle|^2\times\delta(E_M-E_F-\hbar\omega') \quad (2)$$

For adsorbate systems RIXS is the valid description in general.[17,24] However, depending on the particular system, the simpler description of resonantly excited x-ray emission is often applicable. The underlying reason for this is that the valence-electronic structure of chemisorbed molecules on metal surfaces is in many aspects metallic, with a characteristic screening response towards ionization and excitation.[30–34] In these systems, independent of excitation energy, locally the same fully screened core-excited intermediate state is reached, as the excited electron will couple to the continuum of the delocalized metal states during the core-hole lifetime.[28,30,31,33] This fully screened and relaxed core-hole state dominates, and therefore represents a single state $|M\rangle$ in the RIXS process [Eq. (1)]. This allows one to use the simple case of the XE description [Eq. (2)], although more than one virtual orbital was involved in the absorption step. The energy difference between the electronic ground state and the fully screened core-hole state $|M\rangle$ is the x-ray photoemission spectroscopy (XPS) core-level binding energy, which in metallic systems is equivalent to the minimum energy required to promote a core electron to just above the Fermi level.

On $c(2\times2)$CO/Cu(100) we performed resonantly excited XES into the lowest-lying absorption resonance of the adsorbate (the broadened molecular lowest unoccupied molecular orbital), combining a high absorption cross section with a small shake-up probability in the absorption step. Although $c(2\times2)$CO/Cu(100) is rather weakly coupled (adsorption energy 0.7 eV/molecule[27]), its valence electronic structure still has metallic character, and its dynamic response to core-hole creation is characterized by dynamic metallic screening,[28,31] thus making the description of resonantly excited x-ray emission applicable.

However, for adsorbates with very small differences in core-level binding energies or with indistinguishable atomic centers, leading to the near-degeneracy of the symmetry-adapted core orbitals, a full RIXS description is necessary. The implementation of RIXS for these systems, based upon ground-state orbitals, has been developed for adsorbed ethylene and benzene.[17,24] A full RIXS description is also necessary for many periodic systems, i.e., crystals. Here the atomic symmetry-selection rules transform to *k*-selection rules, and the energy dependence of the RIXS spectral distribution contains band-structure information on the joint density of states as momentum is conserved in the coupled

absorption and emission steps.[24,35] In metallic systems the relaxed core-hole intermediate state is a localized state without dispersion (impurity model), encompassing all k values. Consequently, valence states spanning the whole momentum space contribute equally to the XE spectral distribution. Vibrational excitation plays an important role in the coupling of the absorption and emission steps. From free molecules, vibrationally excited intermediate states are known to lead to channel interference, making a full RIXS description necessary.[24,36] On adsorbates, vibrational excitation has been found to be highly photon energy dependent, and indications of full vibrational quenching have been found toward threshold excitation.[37]

In summary, for adsorbates which have atomic centers with well-separated core-level binding energies, and where the valence states are strongly coupled to the metal substrate, a single core-excited intermediate state is reached due to the fast screening response in metallic systems. In this situation RIXS can be simplified to a two-step process of x-ray absorption and resonantly excited x-ray emission in a spontaneous radiative decay. Then the x-ray emission cross section is given according to Fermi's golden rule [Eq. (2)] between the relaxed core-hole intermediate state Ψ_{CH} and the valence-hole final states Ψ_v.

B. X-ray emission and valence-band photoemission

As pointed out in Sec. I, ultraviolet photoemission spectroscopy (UPS) is the most common method for the determination of the occupied electronic states of surface adsorbates on metals. In particular, angle-resolved UPS allows one to determine the dispersion of electronic bands in momentum space.[3] However, angular-resolved UPS usually cannot identify the atomic contributions to a specific valence state. In particular, it is not possible to separate adsorbate valence states overlapping with strong substrate states. On the other hand, XES probes the local electronic structure at a specific atom, and provides an atom-specific and symmetry-selective projection of the occupied valence-electronic structure. XES can therefore be seen as the experimental equivalent to building up the electronic structure as a linear combination of atomic orbitals. XES and angular-resolved UPS emphasize different aspects of the electronic structure, and are in this respect complementary techniques: XES resolves atomic contributions to the valence-electronic structure, but integrates over momentum space, whereas UPS resolves the momentum but integrates over all atomic contributions. Indeed, the information from UPS and XES is easy to relate to each other as both spectroscopies reach a similar valence-hole final state. In UPS this is reached in direct photoionization, and in XES via the radiative decay of the intermediate core-hole state.

III. EXPERIMENT

The XES experiments were carried out at beamline 8.0 at the Advanced Light Source at the Lawrence Berkeley National Laboratory. The 89-period undulator with 5-cm period length produces synchrotron radiation (SR) between 120 and 1500 eV at a ring energy of 1.9 GeV. The SR is monochromatized with a spherical grating monochromator and focused to a spot size from 0.01 to 0.02 mm^2. The flux within this focus is $\sim 10^{13}$–10^{14} photons/s.

The experimental station, built at Uppsala University, consists of two UHV chambers with a base pressure of 5×10^{-11} torr. The preparation chamber contains equipment for sample preparation and characterization: an ion-sputter gun, gas inlet, evaporators, a mass spectrometer and a low-energy electron-diffraction (LEED) system. The copper single crystal was mounted on the sample holder where temperatures between 40 and 1500 K can be achieved.

The Cu(100) crystal was cleaned by cycles of argon-ion sputtering and annealing to 900 K, until a well-ordered LEED pattern was obtained and XPS and x-ray absorption spectroscopy (XAS) showed no contamination. The $c(2 \times 2)$ CO overlayer on Cu(100) was prepared by dosing 2-L CO at 80 K, and was monitored with LEED and the known XPS binding energies.[38] The CO molecules are known to occupy on-top sites.[39]

The analyzer chamber houses an electron analyzer (Scienta SES 200),[40] a grazing-incidence x-ray emission spectrometer[41] and a partial electron yield detector[42] for XAS measurements. The XPS and XES detectors are confocal, with their optical axes perpendicular to the incoming beam, which impinges onto the sample surface in grazing incidence at $5° \pm 2°$ to maximize surface sensitivity. The chamber is rotatable around the optical axis of the incoming beam, allowing for angle-resolved measurements.

The radiation from the undulator has almost complete linear polarization with the electric-field vector $\vec{E}$ in the plane of the storage ring. The orientation of $\vec{E}$ relative to the surface is variable, as the sample can be rotated around the axis of the incoming light. The direction of detection is furthermore variable relative to the orientation of the sample and $\vec{E}$ as the analyzer chamber is rotatable independently around the axis of the incoming beam. We denote as normal-emission geometry the situation where the direction of detection is about 5° off the surface normal. In grazing-emission geometry the direction of detection is switched to 80° off the surface normal, with an otherwise unchanged alignment.

Excitation into the adsorbate $2\pi^*$ resonance is chosen to maximize the absorption cross-section, and in order to minimize many-electron excitations.[43] Highly monochromatic x rays from a tunable source are therefore needed. On the carbon atom a core hole is created through the C $1s$ to $2\pi^*$ transition at 287.5 eV, and an oxygen core-hole is created through the O $1s$ to $2\pi^*$ transition at 533.7 eV.[44] To determine the excitation energy, XAS measurements are performed. The photon energy of the incoming radiation was calibrated from the difference in kinetic energy of photoelectrons excited by light monochromatized in first and second orders of the monochromator. The high primary flux necessary to generate a sufficiently strong XES signal can induce modifications of the adsorbate layer, i.e., desorption, change of the bonding site or dissociation. These changes can be monitored as a change of the XPS signal with time. We therefore scan the sample through the beam at a pace such that no modifications of the adsorbate layer can be seen in XPS before and after the XES measurement. The energy resolutions of both the XES spectrometer and the beamline monochromator have been matched in order to have sufficient flux at reasonable resolution. The resolution is set by

the XES spectrometer with a bandwidth of 0.5 eV for carbon and the oxygen *K*-edge spectra.

IV. THEORETICAL TOOLS

A. Cluster model

The theoretical calculations of the XES spectra were based on CO adsorbed on cluster models of the Cu(100) substrate, and were carried out with the DEMON program[45] which implements orbital-based density-functional theory (DFT). The surface was modeled by a Cu_{50} cluster,[16] where the central Cu_5 subunit was described at the all-electron level and the surrounding atoms described using a one-electron effective core-potential (ECP) developed by Mattsson *et al.*[46]

In the ECP description of the Cu atoms the core, including the 3*d* shell, is described by a static potential, which includes the effects of relaxation and polarization of the 3 *d* orbitals, but which only treats the 4*s* valence electrons explicitly. The all-electron copper atoms were described using the Wachters[47] basis set in an $[8s5p3d]$ contraction with one diffuse *p* function and one *d* function added. The carbon and oxygen are represented in these DFT calculations by the IGLO-III basis set of Kutzelnigg *et al.*[48] The Perdew and Wang (PW91)[49] gradient-corrected functional was used to describe the exchange and correlation potentials.

A critical point of the cluster model is the description of the metal valence band. In particular, the description of the delocalized sp-bands is known to be highly dependent on cluster size,[18,50] whereas the description of the localized *d* band is good. In previous publications[16,18] a good description of the *sp* band was ensured by systematically studying Cu_{14}, Cu_{26}, and Cu_{50} clusters.

To estimate the influence of adsorbate-adsorbate interactions we have used a representation where five CO molecules are chemisorbed on a Cu_{14} cluster model, simulating the $c(2\times2)$ overlayer. The Cu_{14} cluster was treated in an all-electron description of the copper atoms.

B. Calculation of x-ray emission spectra

As described in Sec. II A, the XE spectral distributions for the adsorbate system should be calculated according to Fermi's golden rule [Eq. (2)] as spontaneous dipole transitions between all possible valence-hole final states Ψ_v, and the core-hole state, Ψ_{CH}. In this picture each state must be fully optimized in the appropriate valence- and core-vacancy potentials, respectively. However, this scheme leads to difficulties with nonorthogonal and interacting final states unless all valence-hole states are obtained from the same operator. To simplify the calculations we thus replace both the initial and different final-state potentials with a single potential. In this investigation the ground state potential and the relaxed core-hole transition potential DFT(TP) (half-occupied core hole) have been considered. Thus the Kohn-Sham orbitals of the respective potential are used to represent both the initial core-hole state and the final valence-hole states and the transition is treated as an explicit one-electron transition. The evaluation of the dipole transition moments then simply requires the computation of one-electron states ϕ_i, which in the present case is done using the gradient-corrected DFT formalism. To compare experimental and calculated XES spectra we relate the highest occupied one-electron Kohn-Sham orbital to the experimental Fermi edge, and apply Gaussian broadening of 0.5 eV full width at half maximum (FWHM) to the calculated discrete spectra.

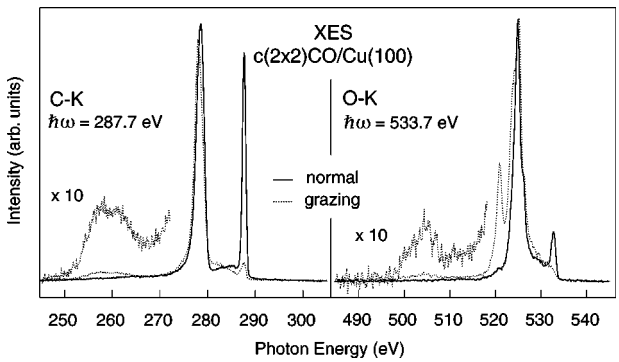

FIG. 1. Resonantly excited x-ray emission spectra on $c(2\times2)$CO/Cu(100). Each spectrum consists of elastically scattered light, conserving the photon energy, and inelastically scattered light.

To discuss core-hole effects, we also use XES transition elements calculated previously in a Hartree-Fock implementation between the fully relaxed core-hole wave function and the ground-state wave function.[18] The Hartree-Fock implementation was chosen for this particular study of relaxation effects as this computational scheme has not been implemented in the DFT code DEMON; all other calculations are at the DFT level. In Ref. 18 the geometry was obtained through energy minimization of CO on a Cu_{13} cluster model with one all-electron copper and the remaining metal atoms described by ECP's. The resulting geometry was R(C-*O*) 1.18 Å and R(Cu-*C*) 1.73 Å, which differs slightly from the R(C-*O*) 1.15 Å and R(Cu-C) 1.86 Å obtained by optimization on an all-electron Cu_{14} cluster. For consistency in the comparison we have performed the DFT XES calculation at both geometries.

V. RESULTS AND DISCUSSION

A. Experimental x-ray emission spectra

In Fig. 1 the experimental XES spectra on $c(2\times2)$CO/Cu(100) are shown. To the left XES spectra obtained at the carbon *K* edge are displayed, and to the right spectra obtained at the oxygen *K* edge. The solid lines are the spectra measured in normal emission to the surface, and the dashed lines are the spectra obtained in grazing-emission geometry. All spectra contain both inelastically and elastically scattered light. The spectral features at 287.7 and 533.7 eV are the elastic contributions, preserving the chosen excitation energy of the C 1*s* to $2\pi^*$ transition and the O 1*s* to $2\pi^*$ transition, respectively. In particular a strong variation of the elastically scattered light with photon energy and angle is found according to the Fresnel description of reflectivity.

Each spectrum is energy calibrated by measuring elastically scattered light from the sample at two different photon energies. (The x-ray spectrometer has a linear dispersion in wavelength, and the photon energy is determined according to Sec. III.) In the next step we subtract the elastic peak from the inelastic contributions, where the peak of the elastically

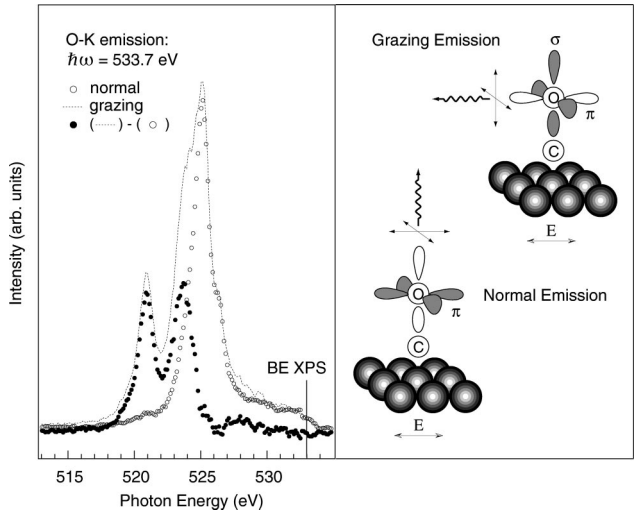

FIG. 2. States of π and σ symmetry are separated by switching the direction of observation between grazing and normal emission. This is illustrated for the O-K spectra of $c(2\times2)$CO/Cu(100).

scattered light is modeled with a Voigt function, approximating the convolution of the monochromator function and the spectrometer function.

Due to the adsorbate order and the symmetry-selection rules of the dipole XE transition, angle-resolved XES spectra yield information on the symmetry of the involved valence states. For K-shell XES on CO/Cu(100), the maximum emission is found perpendicular to the spatial orientation of the involved valence orbitals. Thus switching the direction of detection between grazing emission and normal emission results in the detection of light from p states with different spatial orientation. In normal emission, radiative decay from the atomic p states in the surface plane are strongly selected (molecular π states). In grazing emission, XES from atomic p states in a plane containing the surface normal are detected (molecular σ and π states).

In Fig. 2 we demonstrate the separation of states of π and σ symmetries schematically, and for experimental O-K XES spectra measured in normal- and grazing-emission geometries. Assuming a linear superposition of the π- and σ-derived emissions, a simple subtraction of the scaled normal-emission spectrum from the grazing emission spectrum reveals states of σ-symmeties only. The scaling can be either based on the calculated angular anisotropy of XES, or must be done empirically using known states of pure π and σ symmetry.

In Figs. 3 and 4 the experimental and calculated XES spectra (the DFT ground state) for the oxygen and carbon atoms are shown. Good overall agreement between the ground-state DFT calculations and experiment is found which is the center of the present discussion. The remaining differences will also be discussed in great detail. As our discussion will to some extent treat the relationship between XES and UPS binding energies, we have also included UPS spectra of the $c(2\times2)$CO/Cu(100) from Ref. 51 in direct comparison, but we will begin by concentrating on the experimental XES spectra in Figs. 3 and 4; these have been obtained from the raw spectra in Fig. 1 using the procedure outlined above, and share a common valence binding-energy scale by subtracting the XPS C 1s and O 1s binding energies, respectively. The spectra are normalized within each orbital symmetry to unit area to facilitate the comparison of relative intensities within each spectrum and of the line profiles between carbon and oxygen states.

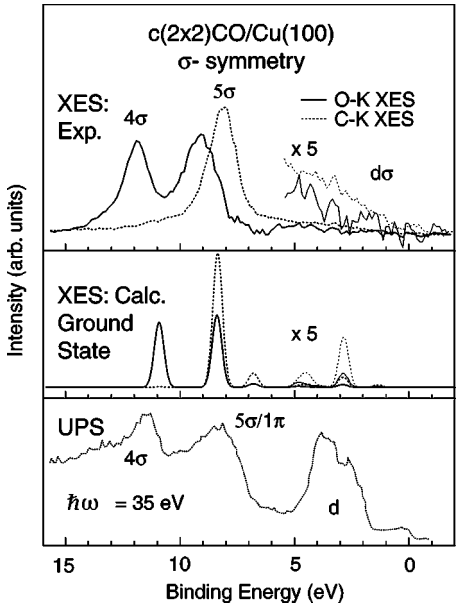

FIG. 3. Compilation of experimental and theoretical results on $c(2\times2)$CO/Cu(100) for states of σ symmetry: (1) Experimental x-ray emission spectra. (2) Calculated x-ray emission spectra in the ground-state approximation on CO/Cu_{50}, with a Gaussian broadening of 0.5 eV FWHM. (3) UPS spectra from Ref. 51.

In the experimental O-K XES representing states of σ symmetry (Fig. 3) two distinct features are found on the oxygen side at 9.0 and 11.8 eV. These are the 5σ and 4σ states, respectively. Their intensity ratio $4\sigma/5\sigma$ is ~0.9, with

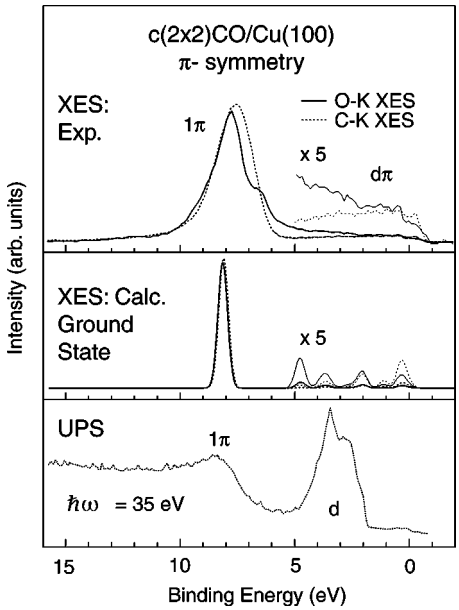

FIG. 4. Compilation of experimental and theoretical results on $c(2\times2)$CO/Cu(100) for states of π symmetry: (1) Experimental x-ray emission spectra. (2) Calculated x-ray emission spectra in the ground-state approximation on CO/Cu_{50}. (3) UPS spectra from Ref. 51.

a variation of ± 0.05, depending on the method of determination (peak heights, areas, curve fits). Some additional intensity extending to the Fermi level is found below 5-eV binding energy. The most prominent state of σ symmetry on the carbon side is the 5σ state at 8.1 eV accompanied by the weak 4σ state at 11.5 eV. The FWHM of the 5σ and 4σ states on the carbon and oxygen sites is about 1.6 eV. In Fig. 3, the inner-valence transitions (3σ) are not included for clarity. However, from the raw data in Fig. 1 we see directly that intensity from the inner-valence region is observed between 25- and 30-eV binding energy in both carbon and oxygen XES (magnified section). Large differences between the carbon and oxygen XES are found, which will be discussed in detail later.

In the π-system the 1π state dominates. In the C-*K* XES its binding energy is 7.5 eV, with a FWHM of 1.8 eV, and in the O-*K* spectrum it is 7.8 eV with a 1.4-eV FWHM. Toward lower binding energies significant differences are found between the carbon and oxygen sites. In the carbon spectrum a weak intensity extends from a cutoff at the Fermi level toward higher binding energy, showing a minimum around 5 eV. On the oxygen side a broad distribution of states is found, with a local maximum around 6.6-eV binding energy. This distribution becomes weaker toward the Fermi level, but preserves an intensity comparable to the carbon states between 2 and 0 eV.

B. Interpretation of x-ray emission intensities

In order to interpret experimental XES spectra in terms of the ground-state valence electronic structure, a relationship between the relative intensities within the XES spectral distribution at each atomic center and the calculated ground-state orbital populations and XES transition elements must be found. The interpretation of XES spectral features is a longstanding issue originating from the application of this spectroscopy to determine the bulk electronic structure of metals.

1. Dynamic core-hole effects

In the interpretation of XES intensities core-hole creation and annihilation play important roles. In particular, the dynamic response due to the creation of the core hole must be considered, as this can lead to substantial effects on the spectroscopic observables. The term ''dynamic effects'' has been coined to summarize the equilibration response of valence electrons to the sudden core-hole creation or annihilation. For homogeneous systems, model calculations on an independent electron gas have been performed.[52–56] In this treatment two extreme cases are computationally accessible: The first case is the short-time limit where the interaction between the core hole and the electron gas is infinitely short. In this case the effects of the presence of the core hole are negligible, and the final-state electronic configuration determines all spectral features which are then calculated as the one-particle transition elements obtained from orbitals calculated in the final-state potential of the x-ray process. The other scenario is the long-time limit. Here the core hole is also annihilated suddenly, but it was present before as a static state. Spectroscopically the latter case is characterized by the occurrence of the Mahan–Nozieres–de Dominicis (MND) x-ray edge divergence or threshold singularity.[53,57,58] As a matter of fact the spectral distributions obtained for the long and short-time limits are related directly, as the spectral distribution obtained in the long-time limit is the spectral distribution of the short-time limit modified by multiplicative exponential threshold singularities, varying for each angular momentum.

2. Final-state rule

The treatment of dynamic core-hole effects as outlined above led to the formulation by von Barth and Grossmann in 1979 (Ref. 54) of the ''dynamic'' final-state rule and the ''static'' final-state rule for the relative XES intensities.

(a) The dynamic final-state rule. The energetic positions and relative intensities in the spectral distribution of XES spectra on simple metals are given by the one-particle transition elements calculated from orbitals in the final-state potential of the x-ray process and multiplicative singularity functions at the Fermi level for each angular momentum, which take care of the dynamic core-hole effects.[54–56,59]

(b) The static final-state rule. As an extension of the dynamic final-state rule, von Barth and Grossmann found that the XES spectra generated by their dynamic calculations are in many cases mimicked rather well by static one-particle transition elements only, calculated from orbitals in the final-state potential of the x-ray process.

Within this thinking the final-state rule was extended to narrow-band metals and varying core-hole strength.[59,60] The influence of dynamic core-hole effects can be categorized depending on the occupation of the valence band. The singularity behavior increases with decreasing occupancy. This means that for nearly empty bands the dynamic effects become large. In the case of highly occupied bands dynamic effects are negligible, and the spectral distribution is given by the one-electron description.[59,60]

As these rules are based on model calculations for a homogeneous and noninteracting electron gas, their applicability depends on how well an interacting electron system is approximated by this model. The valence electronic structure of simple *sp* metals is well approximated by a noninteracting electron gas. Therefore, the final-state rule is directly applicable to the XES spectroscopic results on these systems. For adsorbates on transition metals a description of the valence-electronic structure based on an independent-electron model is questionable; here the adsorbate atoms and the localized *d* states in transition and noble metals are expected to cause large deviations.

With this in mind let us return to the interpretation of the XES relative intensities for CO/Cu. In the top panel of Fig. 5 a computed C-*K* XES of π symmetry is shown, calculated at the Hartree-Fock level as the dipole transition between the relaxed core-hole wave function Ψ_{CH} and the ground state wave function Ψ_{GS}.[18] In this calculation a significant enhancement of states close to the Fermi level is observed which is not seen in the experimental spectrum that is shown for direct comparison in the lower panel of Fig. 5. The poor energy position of the 1π state relative to the Fermi level (taken as the highest occupied orbital for the adsorption model) in the Hartree-Fock calculations is due to the failure of Koopmans' theorem for $3d$ levels; the more appropriate treatment of dynamic correlation in the DFT leads to a more

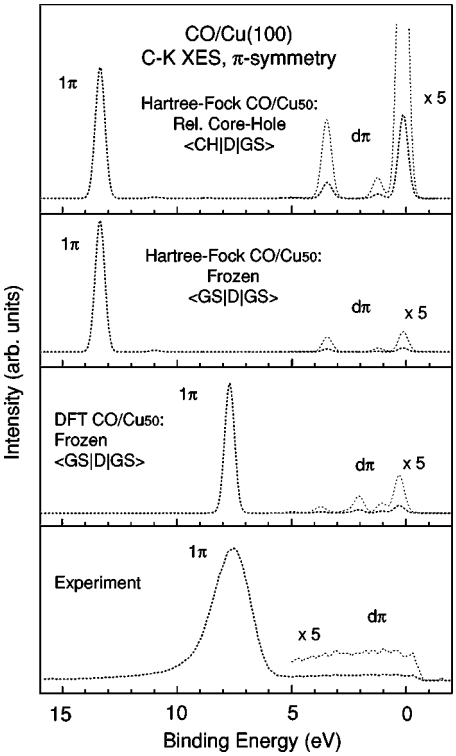

FIG. 5. Comparison of relative intensities in the C-*K* x-ray emission spectra of π symmetry for the experimental spectrum and computed spectra, which are calculated in different approximations. The CO/Cu_{50} cluster has the same geometry in all calculations.

balanced description of the relaxation effects in the different levels and a strongly improved energy separation between levels. All valence-hole final states are described using ground-state molecular orbitals in the calculation. This is correct for independent-electron models and a good approximation for simple metals, and consequently represents the calculation in the long-time limit or the dynamic final-state rule with a threshold singularity as discussed above. However, for interacting electrons valence-hole relaxation may be sizable, and may cause orbital changes similar to those due to the relaxed core hole; using ground-state orbitals to describe the final (valence-hole) state in combination with the fully relaxed core hole may then be a poor approximation. Therefore, it can be anticipated that the neglect of valence-hole relaxation could be the reason for the obvious discrepancy between experiment and the Hartree-Fock calculation with a relaxed core-hole only.

3. Role of valence hole relaxation

In CO/Cu the valence electronic structure involves, to a large extent, the Cu 3*d* states which have large electron correlation effects. One main difference between an independent-electron gas and a correlated electron system is the response to a valence vacancy. The valence-hole relaxation in CO/Cu should vary significantly, and increase with the energy of the valence vacancy. If we consider the energy difference between the ground state and the real valence-hole final state, the valence-hole relaxation can be seen as a correction to the ground-state calculation. The energetics associated with final-state relaxation was calculated at the Hartree-Fock level for the CO/Cu_{14} (Ref. 61) model system, and may be characterized as follows: the metal 3*d* level is very large (5–8 eV), the adsorbate valence levels are large (around 3 eV), and the metal conduction levels are small (0.2–1 eV). It should be noted that the large difference between the 3*d* and adsorbate level relaxations is mainly due to the failure of Koopmans' theorem in the Hartree-Fock calculation, but the trend is intuitively clear, as the relaxation due to a vacancy in an outer-valence state (most extreme, in the highest occupied molecular orbital) is much smaller than for an inner-valence vacancy.

For the discussion of valence-relaxation effects we consider three different approaches, using the experimental and computed C-*K* XES of π symmetry. All the spectra are summarized in Fig. 5. To allow an easy comparison of the relative intensities within each spectrum we have normalized the respective 1π to equal height. The following spectra are presented in Fig. 5.

(1) The already discussed Hartree-Fock calculation (top panel), where the transition moments are calculated between the relaxed core-hole wave function Ψ_{CH} and the ground state wave function Ψ_{GS}.

(2) The frozen-orbital approach. Here both the initial- and final-state wave functions have been calculated within the ground-state potential. In this case core-hole relaxation and valence-hole relaxation are both neglected. This model has been implemented in both Hartree-Fock and DFT (both middle panels) calculations. The latter includes electron correlation.

(3) The experimental spectrum (lower panel). We assume that the experimental spectrum coincides with the hypothetical exact solution, where the transition moments are obtained from the relaxed core-hole wave function Ψ_{CH} and all possible relaxed valence-hole wave functions Ψ_v.

It is directly seen that the calculations which give best agreement with the experimental relative intensities [case (3)] are obtained in the frozen orbital approach [case (2)]. Here we do not observe the significant enhancement of states close to the Fermi level which dominate the calculated spectrum between Ψ_{CH} and Ψ_{GS} in case (1). This suggests that the dynamic core-hole effects are balanced by a variation in final-state relaxation, which is not included in independent-electron models and case 1, or that the excitation-deexcitation process is a true one-step process where relaxation effects are minimal.

Let us now investigate the notion of balance between dynamic core-hole effects and varying valence-hole relaxation by considering the general structure of the XES transition elements according to Fermi's golden rule [Eq. (2)]. The matrix elements between respective initial- and final-state wave functions $|F\rangle$ and $|M\rangle$ are conveniently split into the one-electron dipole transition between the active 1*s* core orbital ϕ_{1s} and each valence orbital ϕ_v. The orbital overlap of all other orbitals, which are not involved in the one-particle transition, results in the codeterminant factor Codet for each ϕ_v:

$$\langle F|\vec{D}|M\rangle \sim \langle \phi_v|\vec{D}|\phi_{1s}\rangle \times \text{Codet}.$$

If both the initial and final states are calculated in the same potential, Codet is constant for all valence-hole final states, and the relative intensities are given by the one-electron transition elements. This is the case in the frozen orbital calculations [case (2)].

The difference between the frozen-orbital calculation and the transitions calculated between Ψ_{CH} and Ψ_{GS} in case (1) is a modification of all one-electron transition elements due to the core-orbital contraction and the response of the valence orbitals to the created core vacancy in the relaxed core-hole wave function Ψ_{CH} in case (1). More important, a strong variation of the Codet toward threshold emphasizes transitions from threshold valence levels strongly over lower-lying valence levels, thus forming a threshold singularity. Note that for gas phase CO the differences between the relaxed and frozen-orbital calculations are very small,[18] while they become very large for CO adsorption on large (polarizable) metal cluster models where electrons for screening the initial- and final-hole states are easily available.

Let us now consider the hypothetical case of calculating the XES transition between all possible relaxed valence-hole final states Ψ_v and the relaxed core-hole state Ψ_{CH} [case (3)]. Here we have not only core-hole effects, but also valence-hole relaxation. The valence-hole relaxation will modify the energetic positions of all valence states (discussed in Sec. V C), but we consider now only the relative intensities. If we assume small changes of the one-electron transition elements in comparison to case (1), where only the core-hole relaxation is included, the difference between these two calculations must be determined by Codet. Consequently, Codet should vary little for the full calculation case (3), which is in contrast to case (1), where Codet varies strongly towards the Fermi level. The reason behind this should be that toward threshold Codet is large due to the x-ray edge divergence, but toward deeper valence holes, where the influence of the threshold singularity decreases, the increasing valence-hole relaxation keeps the magnitude of Codet comparable at a compensating rate.

Consequently, the experimental spectra and the hypothetical exact calculation of the matrix elements between the relaxed core-hole wave function Ψ_{CH} and the different relaxed valence-hole wave functions Ψ_v [case (3)] are approximated very well by calculations with the initial and final states calculated in the same potential, i.e., the ground state [case (2)]. In this case Codet is constant for different valence-hole final states.

Another possibility is to use a transition potential approach (DFT-TP), where the initial and final states are calculated in the same core-hole potential. In the DFT-TP calculation the initial core-ionized state is represented accurately, but all valence orbitals in the final state are evaluated in the presence of the core hole. As in the frozen, orbital approach [case (2)] Codet is also constant. However, in contrast to the ground state calculation the $4\sigma/5\sigma$ ratio in the DFT-TP calculation deviates significantly from experiment (see Table I). As in both the ground-state picture and the relaxed-core-hole picture (DFT-TP) Codet is constant, the difference in the $4\sigma/5\sigma$ ratio must be directly related to the final-state wave function. Therefore, the good agreement between the one-electron ground-state calculation and experiment shows that the experimental XES intensities are a good representation of the ground-state valence electronic structure.

TABLE I. Experimental and computed spectral data for CO chemisorbed on Cu(100). DFT results at optimized geometry for CO on a Cu_{50} cluster model (experimental values from Ref. 79 in parentheses): $r_{CO}=1.15$ Å (1.15 Å) and $r_{CuC}=1.86$ Å (1.90 Å).

	Int. ratio	Binding energy (eV)		
	$4\sigma/5\sigma$	4σ	1π	5σ
Experiment	$\sim 0.90\pm 0.05$ [a]	- [b]-11.8 [a]	7.5 [b] -7.8 [a]	8.1 [b]-9.0 [a]
DFT-Ground	0.90	10.9	8.1	8.4
DFT-core TP	2.77	11.5	8.5	9.2

[a]O-*K* XES
[b]C-*K* XES

In summary, For a balanced treatment of dynamic core-hole effects and valence-hole relaxation either the full calculation of core- and valence-hole relaxation should be performed—if computationally possible—or should not be included at all. In this case the initial and final states must be calculated in the ground state potential.

4. Is RIXS a true one-step process?

Our interpretation of the XES relative intensities has centered around a cancellation of dynamic core-hole effects and valence-hole relaxation. This cancellation, as presented, is rather coincidental and therefore conceptually unsatisfying, especially as the one-electron ground-state model works surprisingly well for a large range of systems, from metals via insulators to free molecules. Experimentally, the core-hole intermediate state is not an observable. We only know that RIXS leads to a valence excitation of an electronic system with an enhanced cross section at core-level thresholds. The formulation of the core-hole intermediate state is, strictly speaking, the construction of the second-order perturbation treatment of the photon-electron interaction. In a true one-step description of the valence excitation in the x-ray scattering process, the agreement with the ground-state model which neglects both core-hole relaxation and valence-hole relaxation would be less puzzling as no core-hole intermediate state would be formed.

C. Interpretation of x-ray emission energies

In XES the energy scale is given by the energy difference between the core-excited state and the valence-hole final state. The energy needed to reach the core-excited intermediate state from the ground state is in general the energy of the absorbed photon. However, as outlined in Sec. II A metallic screening always leads, independent of photon energy, to a fully screened core-excited intermediate state. The XAS onset thus coincides with the XPS core-level binding energy.[28] Subtracting the XPS core-level binding energy from the XES energy scale therefore yields a valence binding-energy scale which measures the energetic difference between the ground state and the valence-hole final states. Consequently, we can put XES spectra from different atomic centers onto a common valence binding-energy scale, where the Fermi level is given by the respective XPS core-

level binding energies. The intermediate core-hole state in XES has therefore no influence on the valence binding energies. Assuming that the same final state is reached in direct valence ionization (UPS) and via the core-hole intermediate state in XES, valence states share a common binding energy scale in UPS and XES.

In Figs. 3 and 4 the XES spectra are directly compared to valence photoelectron spectra.[51] Generally, the overall energetic ordering of spectral features in UPS and XES is comparable. However, there are significant deviations between the binding energies in UPS and XES, most notably in the σ channel (Fig. 3). For example, the 4σ state in XES is shifted ~ 0.5 eV toward lower binding energy than in UPS. We also observe that the ''same'' spectral feature has different binding energies for XES on the carbon and oxygen atoms. The 1π state for C-*K* XES and O-*K* XES differs by ~ 0.3 eV, and the 5σ state even by ~ 1.0 eV. These discrepancies are the subjects of the following sections.

1. Band dispersion

XES resolves atomic contributions to the valence-electronic structure, but integrates in a metallic system over valence-hole final states spanning the whole momentum space. Angle-resolved UPS, on the other hand, separates valence-hole final states of different momenta[62–65] but integrates over all atomic contributions. Therefore discrepancies are expected between the momentum-averaged XES binding energies and the UPS binding energies, selecting a certain momentum interval unless the UPS data have been measured integrating over momentum space, i.e., the first Brillouin zone. The dispersion of valence states is strongly dependent on the CO-CO lattice distance, and in $c(2\times 2)$CO/Cu(100) is approximately 0.5 eV for 4σ and 5σ and approximately 0.2 eV for 1π, whereas dispersion is negligible for lower-lying levels.[66] In our computational modeling band dispersion was investigated by calculations with periodic boundary conditions or by using a Cu_{14} cluster model with five CO molecules, representing the $c(2\times 2)$ overlayer. Here a splitting of valence levels by less than 0.5 eV has been found in comparison to the cluster model with a single adsorbed CO molecule. The $c(2\times 2)$CO/Cu(100) UPS spectra from Ref. 51 in Fig. 4, curve 3 have been taken in the ''forbidden'' and ''allowed'' geometries at 65° off-normal emission. They were recorded in normal incidence at 35 eV with the $\vec{E}$ vector parallel to the $\overline{\Gamma X}$ direction of the Cu(100) crystal. This geometry and energy selects, in $c(2\times 2)$CO/Cu(100) emission, the vicinity of the $\overline{\Gamma}$ point of the second Brillouin zone in the adsorbate, and is moreover characterized by comparable intensities for σ and π states. At the $\overline{\Gamma}$ point the bottom of bands arising from σ states and the top of bands arising from π states are found. Although band dispersion can lead to different binding energies in UPS and XES, this cannot explain the observed differences in Figs. 3 and 4. In comparison to the UPS features the XES σ and π states lie at higher and lower binding energies, respectively, which is opposite to the shifts expected from the band dispersion. Consequently other contributions should cause the observed differences between XES and UPS binding energies.

2. Final-state configuration interaction

As seen in Figs. 3 and 4, differences in binding energies between the experimental XES and UPS spectra are observed, as well as differences for C-*K* and O-*K* XES spectra. The influence of the core hole should be negligible for the binding energy position of spectral features in XES, as reasoned above. Furthermore, the ground-state calculations exhibit no energetic splittings for states projected onto the carbon and oxygen atomic centers. Therefore, the question is whether the properties of the valence-hole final state can generate such a splitting. In the experimental XES spectra (Fig. 1, magnified part), we observe that the 3σ inner-valence level differs significantly for C-*K* XES and O-*K* XES. In the C-*K* spectrum a double-peak structure is observed, spanning ~ 10 eV; in the O-*K* spectrum we observe a single structure, spanning ~ 6 eV. As an inner-valence state the 3σ state has a negligible dispersion which excludes any band-structure effects, and the large differences must therefore solely be due to the fact that the 3σ valence vacancies differ whether they have been created by a dipole decay into the C $1s$ or O $1s$ core hole.

The 3σ valence vacancy in the CO gas molecule is known to be dominated by final-state configuration interaction (CI), where the one-electron molecular-orbital picture cannot describe the experimental observables in UPS.[67–69] In this case the one-electron transitions are accompanied by equally strong multielectron excitations involving the energetic lower-lying outer-valence levels. The UPS spectrum of the CO gas 3σ region consequently has an energy spread of approximately 10 eV, which is preserved upon adsorption and has been observed in UPS measurements of CO on Pd(100).[70] The CI picture can also be seen as the decay of the initial one-electron valence vacancy into lower-lying valence states, leading to a substantial lifetime broadening. For metals the probability for the initial valence hole to decay is approximately proportional to the number of occupied states between the Fermi level and the valence hole. In copper the lifetime broadening of a *d* vacancy is of the order of 100 meV at the top of the *d* band, and increases toward the bottom of the band.[71]

When the initial one-electron valence vacancy cannot decay further via lower-lying valence states, the lifetime becomes very long, leading to a sharp one-electron state. For this reason the CO gas outer-valence states 4σ and 5σ are well-defined one-electron spectral features in UPS.

In the adsorbate all valence levels are coupled to the metal substrate. Due to the absence of a band gap, all one-electron valence states can decay further into multiply excited states involving metal states. Consequently, the adsorbate valence levels are substantially broadened up to 1 eV in both the UPS and XES spectra. On the computational side the simulation of final-state configuration interaction in an adsorbate exceeds the available capabilities. Even for isolated CO the inner valence calculations are difficult.

How are the discussed CI effects manifested in the UPS and XES binding energies? In UPS similar photoionization cross sections are found for the atomic $2s$ and $2p$ contributions,[72] whereas in XES selectively final states of atomic $2p$ character are probed. Thus different aspects of the adsorbate valence-electronic structure are selected in the two

spectroscopies. Assuming that the relative atomic $2s$ and $2p$ contributions vary across the width of the lifetime- or CI-broadened 4σ and 5σ levels, the respective peak maxima should differ in binding energy, since UPS probes both the atomic $2s$ and $2p$ characters whereas XES probes only the local atomic $2p$ character.

A similar mechanism could explain the differences between the O-*K* and C-*K* XES binding energies. The assumption is that the relative atomic $2p$ contributions vary within the broadened valence levels for the different atomic centers, namely, the carbon and oxygen atoms. As XES is a local, atom-specific probe of the local atomic $2p$ contributions, different parts within the broadened valence level will be projected out and XES spectra measured on the carbon and oxygen atomic centers will have different emphases, resulting in binding-energy shifts. This interpretation is also supported by XES spectra from the two chemically inequivalent nitrogen atoms in N_2/Ni(100), where no binding-energy shifts are found in correspondence to the much smaller electronegativity difference within the homonuclear adsorbate.[10]

3. Shake-up

Closely related to the discussion of configuration interaction are shake-up features. Multiple excitations or shake-up are possible in the initial x-ray-absorption step but also in the subsequent XES step. To minimize the former, threshold excitation has been used, effectively creating a single core-excited state as discussed previously in Sec. II A. Shake-up processes in the XE step lead to final-state satellites, which occur toward lower photon energies relative to the one-electron transitions. In general, final-state satellites are a special case of configuration interaction, where the one-particle main line is discernible from the multielectron CI lines. The probability for final-state satellites in XES on bulk metals has been found to be very low,[73] whereas in UPS final-state satellites are commonly observed. In contrast to the bulk metal, in adsorbed CO we monitor valence vacancies which were created by the XES decay into the C $1s$ or O $1s$ core holes located on the adsorbate. The question is whether in this case the final-state shake-up probability becomes higher than in bulk metal. In this context we focus onto the adsorbate states derived from the metal *d* band between 0- and 7-eV binding energies. These states are nearly pure metallic states with only small molecular contributions. The lower-lying valence-states 3σ, 4σ, 5σ, and 1π have already been discussed in terms of CI and lifetime broadening as no discrete shake-up features to them are observed (Figs. 1, 3, and 4). In general, a *d*-band vacancy can be itinerant (delocalized) or localized to a particular site.[74–78] Spectral features due to itinerant valence holes mimic the *d*-band partial density of states. In contrast, localized *d* vacancies lead to deviations in energy, forming satellites. The d-vacancy localization energies are 3.6 and 3.1 eV for Cu and Ni, respectively.[78] In the O-*K* XES spectra of π symmetry a shoulder at 6.6 eV is observed which is not seen in the calculated ground-state d_π band which lies between 3 and 5 eV (Fig. 4). A similar structure was also seen in the O-*K* XES of π symmetry in CO on Ni at 4.5 eV, which is also not seen in the ground-state calculations.[7,19] A possible interpretation of these features could be final-state shake-up in the d_π band. In both cases these energies are approximately in agreement with the experimentally observed shifts which suggests a shake-up interpretation for the adsorbate d_π band. Indeed the probability of reaching a localized or itinerant *d* valence hole is element specific. With increasing contraction of the *d* shell going along the transition-metal row the electron correlation and the probability of *d* hole localization increase. Cu is the first noble metal after the $3d$ transition metals. The probability of *d*-hole localization is therefore higher in Cu than in Ni, and the XE spectral distribution deviates more strongly from the partial density of states, represented by the itinerant *d* holes. In the molecularlike states 1π, 5σ, and 4σ, these effects are expected to be much smaller.

4. Vibrational excitation

So far we have discussed the observed spectral features solely in terms of electronic transitions and excitations. Additionally, vibrational motion has to be taken into account which is excited due to the rapid change of the molecular potential in the photon-electron interaction. Although our experiment is far from resolving vibrational fine structure on adsorbates, vibrational excitation is expected to influence the width and energetic position of the spectral features through different vibrational envelopes. Different vibrational envelopes are due to the fact that, in UPS, the potential-energy surfaces of the ground state and the valence-hole final state define the vibrational excitation or the vibrational envelope, whereas in XES additionally the potential-energy surface of the respective C $1s$ or O $1s$ core-hole intermediate state is involved, leading to deviations between UPS and C-*K* and O-*K* XES spectral features. In general, the degree of vibrational excitation varies considerably for the different atomic centers which is, e.g., seen in the O $1s$ and C $1s$ XPS vibrational envelopes with full widths at half maximum of 1.7 and 0.7 eV, respectively.[30,31] As pointed out in Sec. II A, vibrational excitation in the absorption-step makes in general a full RIXS description necessary due to the occurence of lifetime vibrational interference (LVI) between the vibrational states reached in the core-hole intermediate state. In gas-phase molecules LVI leads to a strong redistribution of spectral intensity toward higher binding energies which is seen as the vibrational envelopes deviate from the Franck-Condon behavior.[24,36] Similar effects for the adsorbate can modify the XES binding energies between carbon and oxygen, and can also introduce deviations in comparison to UPS. However, for adsorbed CO there are indications of vibrational quenching for threshold-excitation,[37] making a simple XE description applicable. In the calculated XE spectra, vibrational effects have not been included.

VI. SUMMARY

In summary we have reviewed the experimental, analytical, and theoretical tools associated with resonantly excited x-ray emission spectroscopy on CO adsorbed on Cu(100). This system stands as an example for adsorbates with no equivalent atomic centers on transition and noble metals, where the valence electronic structure is characterized by strong interaction with the metal substrate. Here the spectral distribution of resonant inelastic x-ray scattering is well described as spontaneous resonantly excited x-ray emission. The absorption and emission steps become independent of

each other due to the fast screening response in the metallic system and the symmetry properties of these adsorbates. By switching the direction of observation the symmetry of the involved states is revealed. The experimental spectral distribution can be modeled successfully by frozen-orbital ground-state calculations which represent just the most simple one-electron picture of a passive core hole into which the ground-state valence electrons decay. The observed agreement suggests that relaxation effects have a negligible influence in this spectroscopy, which could be due to a cancellation of dynamic core-hole effects and valence-hole relaxation; this can only be tested by further development of the theoretical techniques to include the fully relaxed valence-hole final states. This, however, is beyond the present capabilities for surface adsorbed systems. Another interpretation is that the inelastic x-ray scattering process is a true one-step process without the formation of a relaxed core-hole intermediate state and small differential final-state effects. From the present investigation, and from earlier studies on a large number of diverse adsorbate systems,[10,14–22] it is clear that the frozen ground-state orbitals give the best representation so far of the spectral features of XES. Under these circumstances XES is a measure of the valence-electronic structure in an atom-specific and orbital-symmetry-selective projection onto the respective core orbitals. Finally, agreement between experimental and calculated XES can be used to assess the quality of theoretical models which are the basis to interpret the ground-state electronic structure of the adsorbate and local bond characteristics.

ACKNOWLEDGMENTS

This work was supported by the Swedish Natural Science Research Council (NFR) and by the Göran Gustafsson Foundation for Research in Natural Science and Medicine. The valuable support of N. Mårtensson, J. Nordgren, and J. Stöhr is gratefully acknowledged. H. Ågren is acknowledged for many valuable discussions.

*Author to whom correspondence should be addressed. Electronic address: alexander.foehlisch@fysik.uu.se

[1] G. A. Somorjai, *Surface Chemistry and Catalysis* (Wiley, New York, 1994).

[2] *The Chemical Physics of Solid Surfaces and Heterogeneous Catalysis*, edited by D. A. King and D. P. Woodruff (Elsevier, New York, 1981), Vols. 1–6.

[3] H.-J. Freund and H. Kuhlenbeck, in *Application of Synchrotron Radiation*, edited by W. Eberhardt, Springer Series in Surface Sciences Vol. 35 (Springer, Heidelberg, 1994).

[4] N. Wassdahl, A. Nilsson, T. Wiell, H. Tillborg, L. Duda, J. H. Guo, N. Mårtensson, J. Nordgren, J. N. Andersen, and R. Nyholm, Phys. Rev. Lett. **69**, 812 (1992).

[5] H. Tillborg, A. Nilsson, T. Wiell, N. Wassdahl, N. Mårtensson, and J. Nordgren, Phys. Rev. B **47**, 16 464 (1993).

[6] T. Wiell, H. Tillborg, A. Nilsson, N. Wassdahl, N. Mårtensson, and J. Nordgren, Surf. Sci. **304**, L451 (1994).

[7] A. Nilsson, P. Bennich, T. Wiell, N. Wassdahl, N. Mårtensson, J. Nordgren, O. Björneholm, and J. Stöhr, Phys. Rev. B **51**, 10 244 (1995).

[8] A. Nilsson, M. Weinelt, T. Wiell, P. Bennich, O. Karis, N. Wassdahl, J. Stöhr, and M. Samant, Phys. Rev. Lett. **87**, 2847 (1997).

[9] A. Nilsson, N. Wassdahl, M. Weinelt, O. Karis, T. Wiell, P. Bennich, J. Hasselström, A. Föhlisch, J. Stöhr, and M. Samant, Appl. Phys. A: Solids Surf. **65**, 147 (1997).

[10] P. Bennich, T. Wiell, O. Karis, M. Weinelt, N. Wassdahl, A. Nilsson, M. Nyberg, L.G.M. Pettersson, J. Stöhr, and M. Samant, Phys. Rev. B **57**, 9274 (1998).

[11] A. Nilsson, J. Electron Spectrosc. Relat. Phenom. **93**, 143 (1998).

[12] T. Wiell, J. E. Klepeis, P. Bennich, O. Björneholm, N. Wassdahl, and A. Nilsson, Phys. Rev. B **58**, 1655 (1998).

[13] M. Weinelt, N. Wassdahl, T. Wiell, O. Karis, J. Hasselström, P. Bennich, A. Nilsson, J. Stöhr, and M. Samant, Phys. Rev. B **58**, 7351 (1998).

[14] J. Hasselström, A. Föhlisch, O. Karis, N. Wassdahl, M. Weinelt, A. Nilsson, M. Nyberg, L.G.M. Pettersson, and J. Stöhr, J. Chem. Phys. **110**, 4880 (1999).

[15] M. Staufer, U. Birkenheuer, T. Belling, F. Nörtemann, N. Rösch, M. Stichler, D. Menzel, W. Wurth, L.G.M. Pettersson, A. Föhlisch, and A. Nilsson, J. Chem. Phys. **111**, 4704 (1999).

[16] L. Triguero, L.G.M. Pettersson, and H. Ågren, J. Phys. Chem. A **102**, 10 599 (1998).

[17] L. Triguero, Y. Luo, L.G.M. Pettersson, H. Ågren, P. Väterlein, M. Weinelt, A. Föhlisch, J. Hasselström, O. Karis, and A. Nilsson, Phys. Rev. B **59**, 5189 (1999).

[18] V. Carravetta, L.G.M. Pettersson, O. Vahtras, and H. Ågren, Surf. Sci. **369**, 146 (1996).

[19] A. Föhlisch, M. Nyberg, P. Bennich, L. Triguero, J. Hasselström, O. Karis, L.G.M. Pettersson, and A. Nilsson, J. Chem. Phys. **112**, 1946 (2000).

[20] A. Föhlisch, M. Nyberg, J. Hasselström, O. Karis, L. G. M. Pettersson and A. Nilsson, Phys. Rev. Lett. (to be published).

[21] O. Karis, J. Hasselström, N. Wassdahl, M. Weinelt, A. Nilsson, M. Nyberg, L. G. M. Pettersson, J. Stöhr and M. Samant, J. Chem. Phys. (to be published).

[22] M. Nyberg, L. G. M. Pettersson, O. Karis, J. Hasselström, N. Wassdahl, M. Weinelt, and A. Nilsson, J. Phys. Chem. (to be published).

[23] H. Ågren, V. Carravetta, O. Vahtras, and L.G.M. Pettersson, Theor. Chem. Acc. **97**, 14 (1997).

[24] F. Gel'mukhanov and H. Ågren, Phys. Rep. **312**, 87 (1999).

[25] J.C. Slater, Adv. Quantum Chem. **6**, 1 (1972).

[26] J. C. Slater and K.H. Johnsson, Phys. Rev. B **5**, 844 (1972).

[27] J. C. Tracy, J. Chem. Phys. **56**, 2748 (1972).

[28] H. Tillborg, A. Nilsson, and N. Mårtensson, J. Electron Spectrosc. Relat. Phenom. **62**, 73 (1993).

[29] J. Sakurai, *Advanced Quantum Mechanics* (Addison Wesley, Menlo Park, CA, 1967).

[30] A. Föhlisch, N. Wassdahl, J. Hasselström, O. Karis, D. Menzel, N. Mårtensson, and A. Nilsson, Phys. Rev. Lett. **81**, 1730 (1998).

[31] A. Föhlisch, J. Hasselström, O. Karis, D. Menzel, N. Mårtensson, and A. Nilsson, J. Electron Spectrosc. Relat. Phenom. **101-103**, 303 (1999).

[32] A. Sandell, O. Björneholm, A. Nilsson, B. Hernnäs, J. Andersen, and N. Mårtensson, Phys. Rev. B **49**, 10 136 (1994).

[33] C. Keller, M. Stichler, G. Comelli, F. Esch, S. Lizzit, W. Wurth, and D. Menzel, Phys. Rev. Lett. **80**, 1774 (1998).

[34] A. Nilsson, O. Björneholm, E. Zdansky, H. Tillborg, N. Mårtens-

son, J. Andersen, and R. Nyholm, Chem. Phys. Lett. **197**, 12 (1992).
[35] Y. Ma, N. Wassdahl, P. Skytt, J. Guo, J. Nordgren, P. D. Johnson, J.-E. Rubensson, T. Böske, W. Eberhardt, and S. D. Kevan, Phys. Rev. Lett. **69**, 2598 (1995).
[36] P. Skytt, P. Glans, K. Gunnelin, J.-H. Guo, and J. Nordgren, Phys. Rev. A **55**, 146 (1997).
[37] A. Föhlisch, J. Hasselström, O. Karis, P. Väterlein, N. Mårtensson, A. Nilsson, C. Heske, M. Stichler, C. Keller, W. Wurth, and D. Menzel, Chem. Phys. Lett. **315**, 194 (1999).
[38] A. Sandell, P. Bennich, A. Nilsson, B. Hernnäs, O. Björneholm, and N. Mårtensson, Surf. Sci. **310**, 16 (1994).
[39] P. Uvdal, P.-A. Karlsson, C. Nyberg, S. Andersson, and N. V. Richardson, Surf. Sci. **202**, 167 (1988).
[40] N. Mårtensson, P. Balzer, P. Brühwiler, J.-O. Forsell, A. Nilsson, A. Stenborg, and B. Wannberg, J. Electron Spectrosc. Relat. Phenom. **70**, 117 (1994).
[41] J. Nordgren, G. Bray, S. Cramm, R. Nyholm, J.-E. Rubensson, and N. Wassdahl, Rev. Sci. Instrum. **60**, 1690 (1989).
[42] J. Stöhr, *NEXAFS Spectroscopy* (Springer-Verlag, Heidelberg, 1992).
[43] P. Bennich, Ph.D. thesis, Uppsala University, 1996.
[44] O. Björneholm, A. Nilsson, E. Zdansky, A. Sandell, B. Hernnäs, H. Tillborg, J. Andersen, and N. Mårtensson, Phys. Rev. B **46**, 10 353 (1992).
[45] deMon-KS version 4.0, M. E. Casida, C. Daul, A. Goursot, A. Koester, L. G. M. Pettersson, E. Proynov, A. St-Amant, D. R. Salahub principal authors, H. Duarte, N. Godbout, J. Guan, C. Jamorski, M. Leboeuf, V. Malkin, O. Malkina, M. Nyberg, L. Pedocchi, F. Sim, L. Triguero, and A. Vela, contributing authors, deMon Software, 1997.
[46] A. Mattsson, I. Panas, P. Siegbahn, U. Wahlgren, and H. Åkeby, Phys. Rev. B **36**, 7389 (1987).
[47] A. J. H. Wachters, J. Phys. Chem. **52**, 1033 (1970).
[48] W. Kutzelnigg, U. Fleischer, and M. Shindler, *NMR-Basic Principles and Progress* (Springer, Heidelberg, 1990), Vol. 23, p. 165.
[49] J. P. Perdew and Y. Wang, Phys. Rev. B **45**, 13 244 (1992); J. P. Perdew, in *Electronic Structure of Solids*, edited by P. Ziesche and H. Eischrig (Akademie Verlag, Berlin, 1991); J. P. Perdew, J. A. Chevary, S. H. Vosko, K. A. Jackson, M. R. Pederson, D. J. Singh, and C. Fiolhais, Phys. Rev. B **46**, 6671 (1992).
[50] K. Hermann, P. S. Bagus, and C. J. Nelin, Phys. Rev. B **35**, 9467 (1987).
[51] D. Heskett, I. Strathy, E. W. Plummer, and R. A. de Paola, Phys. Rev. B **32**, 6222 (1985).
[52] B. Roulet, J. Gavoret, and P. Nozieres, Phys. Rev. **178**, 1072 (1969).
[53] P. Nozieres and C. de Dominicis, Phys. Rev. **178**, 1097 (1969).
[54] U. von Barth and G. Grossmann, Solid State Commun. **32**, 645 (1979).
[55] U. von Barth and G. Grossmann, Phys. Scr. **21**, 580 (1980).
[56] U. von Barth and G. Grossmann, Phys. Rev. B **25**, 5150 (1982).
[57] G. Mahan, Solid State Phys. **29**, 75 (1974).
[58] D. Pines and P. Nozieres, *The Theory of Quantum Liquids* (Benjamin, New York, 1966).
[59] V. I. Grebennikov, Y. A. Babanov, and O. B. Sokolov, Phys. Status Solidi B **79**, 423 (1977).
[60] V. I. Grebennikov, Y. A. Babanov, and O. B. Sokolov, Phys. Status Solidi B **80**, 73 (1977).
[61] J.-L. Pascual, L. G. M. Pettersson, and H. Ågren, Phys. Rev. B **56**, 7716 (1997).
[62] K. Horn, A. M. Bradshaw, K. Hermann, and I. P. Batra, Solid State Commun. **31**, 257 (1979).
[63] F. Greuter, D. Heskett, E. W. Plummer, and H.-J. Freund, Phys. Rev. B **27**, 7117 (1983).
[64] H. Kuhlenbeck, H. B. Saalfeld, U. Buskotte, M. Neumann, H.-J. Freund, and E. W. Plummer, Phys. Rev. B **39**, 3475 (1989).
[65] K. Horn, A. M. Bradshaw, and K. Jacobi, Surf. Sci. **72**, 719 (1978).
[66] S.-S. Sung and R. Hoffmann, J. Am. Chem. Soc. **107**, 578 (1985).
[67] J. Schirmer, L. Cederbaum, W. Domcke, and W. von Nissen, Chem. Phys. **26**, 149 (1977).
[68] L. Cederbaum and W. Domcke, Adv. Chem. Phys. **30**, 205 (1977).
[69] H. Köppel, W. Domcke, and L. Cederbaum, Adv. Chem. Phys. **57**, 59 (1984).
[70] A. Sandell, O. Björneholm, J. Andersen, A. Nilsson, E. Zdansky, B. Hernnäs, U. Karlsson, R. Nyholm, and N. Mårtensson, J. Phys.: Condens Matter **6**, 10 659 (1994).
[71] H. Petek, H. Nagano, and S. Ogawa, Phys. Rev. Lett. **83**, 832 (1999), and references therein.
[72] J. Yeh and I. Lindau, At. Data Nucl. Data **32**, 1 (1985).
[73] N. Wassdahl, J. Rubensson, G. Bray, P. Glans, P. Bleckert, R. Nyholm, S. Cramm, N. Mårtensson, and J. Nordgren, Phys. Rev. Lett. **64**, 2807 (1990).
[74] S. Hüfner, *Photoelectron Spectroscopy* (Springer, Berlin, 1995).
[75] T. Uozumi, K. Okada, A. Kotani, O. Durmeyer, J. Kappler, E. Beaurepaire, and J. Parlebas, Europhys. Lett. **18**, 85 (1992).
[76] D. de Boer, C. Haas, and G. Sawatzky, Phys Phys. Rev. B **29**, 4401 (1984).
[77] S. Hüfner and G. Wertheim, Phys. Lett. **51A**, 299 (1975).
[78] N. Mårtensson and B. Johansson, Phys. Rev. B **45**, 482 (1980).
[79] C. McConvill, D. Woodruff, K. Prince, G. Paolucci, V. Chab, M. Surman, and A. Bradshaw, Surf. Sci. **166**, 221 (1986).